4. M. I. Starovikov, A. I. Drozhzhin, S. A. Antipov, and A. M. Velikov, "Study by direct methods of dislocation structures in silicon WC in the initial stage of plasticity," Dep. VINITI 16.06.83, Voronezh (1983).
5. A. M. Kosevich, Dislocations in Elasticity Theory [in Russian], Naukova Dumka, Kiev (1978).
6. L. D. Landau and E. M. Lifshits, Elasticity Theory [in Russian], Nauka, Moscow (1987).
7. J. Eshelby, Continuum Theory of Dislocations [Russian translation], IL, Moscow (1963).
8. Yu. A. Amenzade, Elasticity Theory [in Russian], Maarif, Baku (1968).
9. R. De Wit, Continuum Theory of Dislocations [Russian translation], Mir, Moscow (1977).
10. S. R. De Groot and L. G. Suttorp, Foundations of Electrodynamics [Russian translation], Nauka, Moscow (1982).

NUMERICAL STUDIES OF NONLINEAR WAVE PROCESSES IN A LIQUID AND A DEFORMABLE SOLID DURING HIGH-SPEED IMPACT INTERACTION

V. A. Petushkov

UDC 532.529+539.4

Problems of hydrodynamic shock loading of deformable bodies are most often encountered in the study and prevention of the erosional failure of structures interacting with a liquid. Among the structures that are subject to high-speed shock loading by liquid particles are turbine blades operating in moist vapor and elements of air and space craft flying in rain or entering bodies of water. Bodies immersed in a cavitating liquid are also subjected to shock-wave loading. The local pressures on the surface of solids involved in such interactions may exceed thousands of atmospheres [1]. There is yet another interesting aspect of such problems – the need to intensify the destructive effects achieved in the hydrodynamic extraction of minerals and fracture of rocks and the development of progressive new methods of cutting materials.

In order to protect structures from failure and select the proper materials and coatings, it is necessary to perform a detailed analysis of their deformation and fracture with different rates of interaction with liquids. The capabilities of empirical methods are extremely limited, since these interactions are of a drop- or jet-mediated nature (with the jets being of the shaped charge type) and are highly localized – with a duration measured in microseconds. The results that have been obtained through experimentation are for the most part qualitative. Only the ablation rate in such interactions provides quantitative data from such studies [1, 2]. The possibilities of theoretical investigations are even more limited. In mathematical modeling the high-speed impact interaction of bodies with a liquid, it is necessary to consider the compressibility of the media, the propagation of shock waves (SW) in them, the nonlinear behavior of the materials (dependent on the loading rate), and the resistance of the materials to plastic shears. The presence of the free surface of the liquid – which changes during the interaction – complicates the solution of the problem [2, 3].

Only a small number of studies [2, 4-6, etc.] have numerically investigated features of the nonlinear deformation and fracture of bodies in such interactions with a liquid. All of them are based on simplifying assumptions made relative to the behavior of the media. However, as was noted in [7], the use of such assumptions makes it possible to determine features of flow in the liquid that are important in determining the loading, deformation, and mode of failure of the given body. The most thorough studies of the dynamics of a drop liquid were made in [7], although they were limited to modeling flows in a liquid in the case of a collision with a nondeformable surface.

The present investigation, being a continuation of [8, 9], numerically examines wave processes in a drop liquid and a deformable body during their high-speed collision. The results are obtained with allowance for the above-mentioned features of the behavior of the media on the basis of the finite differences method and a through computing scheme of the Lachs–Vandroff predictor-corrector type. The Boris–Book flux correction method [10] is

---

Moscow. Translated from Zhurnal Prikladnoi Mekhaniki i Tekhnicheskoi Fiziki, No. 2, pp. 134-143, March-April, 1991. Original article submitted March 6, 1989; revision submitted June 9, 1989.

used to eliminate oscillations in the solution at the boundary of the contact discontinuity and shock-wave fronts in the liquid.

1. Mathematical Model. Basic Equations. A liquid interacting with the surface of a deformable body at high speed will be examined in the form of small spherical particles. The proposed approach can also be used to study thin jets formed due to the collapse of cavitation bubbles in a liquid near the surface of a body and to examine the action of high-pressure nozzles. The forces from the liquid side will be assumed to be directed along a normal to the surface of the body. Ignoring the effect of surface tension and body forces in the liquid, we write the equations of unsteady motion of a compressible fluid in a two-dimensional axisymmetric approximation

$$\rho_{,t} + \operatorname{div} \rho\mathbf{v} = 0, \quad (\rho\mathbf{v})_{,t} + \operatorname{div} (\rho\mathbf{v}\mathbf{v} + \sigma) = 0, \qquad (1.1)$$
$$e_{,t} + \operatorname{div} (e + \sigma)\mathbf{v} = 0, \quad (x^\alpha, t) \in D_1 \times D_t, \ \alpha = 1, 2.$$

Here, $\mathbf{v} = (v_1, v_2)$ is the velocity vector; x^1 and x^2 are the space coordinates (x^2 is the axis of symmetry); ρ is density; $\sigma = -p\mathbf{I}$; p is pressure; $\mathbf{I}$ is the unit tensor; e is the total energy per unit volume of the liquid [$e = \rho\varepsilon + (1/2)\rho(v_1^2 + v_2^2)$].

Written in conservation form system (1.1) is closed by the equation of state

$$p = A(\rho/\rho_0 - 1) + B(\rho/\rho_0 - 1)^2 - C\rho\varepsilon, \qquad (1.2)$$

where A, B, and C are coefficients chosen on the basis of the best approximation of the Hugoniot curve. We take the results presented in [7] for water. Since high-pressure regions in the liquid may coexist with cavitation cavities formed under the influence of negative pressures, we augment the corrected equation of state as follows:

$$p = A(\rho/\rho_0 - 1) \ \text{ at } \ p > -p_*, \ p = p_* \ \text{ at } \ p < p_* \qquad (1.3)$$

(p_* is the maximum negative pressure that the liquid can withstand without loss of continuity. Its value for water does not exceed 28 MPa [7]).

At the initial moment of time, the density, velocity, pressure, and energy of the liquid are determined by the relations

$$\rho = \rho_0, \ v_1 = 0, \ v_2 = u_0, \ p = p_0, \ e = e_0. \qquad (1.4)$$

At the surface of the contact discontinuity with the body being deformed, all data for which have index 2, we introduce the condition of continuous pressure and normalize the components of the velocity $\mathbf{v}$:

$$\mathbf{v}^{(1)}\mathbf{n} = \mathbf{v}^{(2)}\mathbf{n}, \ p_n^{(1)} = p_n^{(2)}. \qquad (1.5)$$

By virtue of the local character of interaction with the liquid, the fact that the diameter of the drops is 2R, and the fact that the diameter of the jet usually is no greater than several millimeters, the body being deformed is usually examined in the form of a half-space with presumed axial symmetry undergoing a normal collision with the liquid. The body is regarded as the most heavily damaged material in the collision. The boundaries of the theoretical region occupied by the deformable medium are chosen at such a distance from the region of impact with the liquid that perturbations which arise near these boundaries are not transmitted inside the region. We will describe the motion of the compressible deformable medium using Eqs. (1.1), but with allowance for the shear stresses. Here, the expression for the stress tensor σ is

$$\sigma_{jk} = -p\delta_{jk} + S_{jk} \quad (j, k = 1, 2, 3) \qquad (1.6)$$

(S_{jk} is the stress deviator). The time derivatives of the components of the deviator in cylindrical coordinates appear as

$$\begin{aligned} \partial S_{11}/\partial t &= 2\mu(\partial v_1/\partial x^1 + (1/3)\rho\partial\rho/\partial t), \\ \partial S_{22}/\partial t &= 2\mu(\partial v_2/\partial x^2 + (1/3)\rho\partial\rho/\partial t), \\ \partial S_{\theta\theta}/\partial t &= 2\mu(v_1/x^1 + (1/3)\rho\partial\rho/\partial t), \\ \partial S_{12}/\partial t &= \mu(\partial v_1/\partial x^2 + \partial v_2/\partial x^1) \end{aligned} \qquad (1.7)$$

and are used in the Jauman–Noll sense [11]

$$S_{jk}^{\nabla} = \dot{S}_{jk} - S_{jr}\Omega_{rk} - S_{kr}\Omega_{rj}, \qquad (1.8)$$

where $\dot{S}_{jk}$ is the total derivative of the Cauchy stresses with respect to time; the vorticity tensor $\Omega_{jk} = (1/2)(v_{j,k} - v_{k,j})$; $v_{j,k} = \partial v_j/\partial x_k$, $x_k \in D_2$.

As the equation of state for the spherical component of the stress tensor (1.6) – the hydrostatic pressure p – investigators usually use relations from the Mie–Gruneisen theory

$$p(v, e) = p_-(v) + p_+(v, e)$$
$$(e = e_+ + e_-,\ p_+ = \Gamma e_+/v,\ p_- = -de_-/dv). \tag{1.9}$$

Here, Γ is the Gruneisen coefficient; p_- and e_- are components of the pressure and energy associated with cold compression of the body; p_+ and e_+ are the same, respectively, with allowance for the heating of the body; $v = V/\rho$ is the specific volume.

Equations (1.9) are established from tests involving shock compression [12] which for most metals indicate a nearly linear dependence of Γ on v, i.e., $\Gamma(v) = \Gamma_0 v/v_0$. Below, we will restrict ourselves to the so-called quasiacoustic approximation – when pressure is a function only of volume and the Hugoniot curve coincides with the isentropic expansion. Such an approximation has been empirically substantiated for a fairly wide range of pressures at SW fronts, on the order of 10-15 GPa [12, 13]. In this range, the irreversibility of the deformation processes is due mainly to plastic shear strains.

To express the connection between the deviatoric components of the stresses S_{jk} and strains e_{jk} ($e_{jk} = \varepsilon_{jk} - (1/3)\varepsilon_{ii}\delta_{jk}$), we will use relations from the theory of microplastic strains in the form in which they appeared in [13, 14]. Here, as in [15], we will generalize them to account for the effect of strain rate. In accordance with this approach, each elementary volume of the body is assumed to consist of n ideal elastoplastic subelements having different yield points dependent on the loading rate:

$$\sigma_{iD}^{(k)} = \sigma_0^{(k)}\left(1 + |C\dot{e}_i|^p\right),\ k \in (1, n), \tag{1.10}$$

where $\sigma_0^{(k)}$ is the static yield point of the k-th subelement; C and p are coefficients determined from stress–strain curves constructed for single loadings at different loading rates and, when necessary, different temperatures. All of the subelements are characterized by the same elastic moduli E and same total strain rates $\dot{\varepsilon}_{jk} = (1/2)(v_{j,k} + v_{k,j})$. Thus, for each subelement k $S_{jk}^{(k)} = 2\mu e_{jk}$ and $(S_{jk}^{(k)})^2 \leqslant \left((2/3)\sigma_{iD}^{(k)}\right)^2$. The total stress deviator at a point – in an elementary volume – is distributed with the corresponding weight factors Ψ(k) between all n subelements, i.e.,

$$S_{jk} = \sum_{(k)=1}^{n} \Psi_{(k)} S_{jk}^{(k)}. \tag{1.11}$$

We can similarly represent the total deviator of plastic strain rate. The weight factors are determined on the basis of a linear approximation of the above-indicated stress–strain curves: $\Psi(k) = (1/E_1)(E_k - E_{k-1})$, where $E_k = (\sigma_i^k - \sigma_i^{k-1})/(\varepsilon_i^k - \varepsilon_i^{k-1})$, while $\sum_{k=1}^{n} \Psi_k = 1$. Such a description of the nonlinear behavior of materials makes it possible to account for ductility-property anisotropy and hysteresis losses due to plastic strains – although an additional 2n parameters Ψ_k and σ_i^k are added to the existing expressions. As has been shown by numerical studies conducted for different structural metals, the optimum number of parameters is never greater than 8-16 subelements (four are usually sufficient) and can be established on the basis of histograms of the yield points of a material [16].

Conditions (1.5) are assigned at the boundary of the theoretical region $S_1 \subset D_2 = \{(x^1, x^2): 0 \leqslant x^1 \leqslant 3R;\ x^2 = 0\}$ (free surface or surface of contact discontinuity) of the deformable body. The following conditions are assigned on the remaining boundaries:

$$\begin{aligned} &v_1 = \partial v_2/\partial x^1 = 0, && (x^1, x^2) \in S_2 = \{x^1 = 0,\ 0 \leqslant x^2 \leqslant 3R\};\\ &\partial v_1/\partial x^1 = \partial v_2/\partial x^2 = 0, && (x^1, x^2) \in S_3 = \{0 \leqslant x^1 \leqslant 3R,\ x^2 = 3R\};\\ &\partial v_1/\partial x^1 = \partial v_2/\partial x^1 = 0, && (x^1, x^2) \in S_4 = \{x^1 = 3R,\ 0 \leqslant x^2 \leqslant 3R\}. \end{aligned} \tag{1.12}$$

The above relations for the deformable body must be augmented by initial conditions. The initial state of the body may either be stress-free or may include "initial" stresses from the main service load (preceding the loading by the liquid) or processing. As for the liquid, we take initial conditions in the form

$$\rho(x^\alpha, 0) = \rho_0,\ v_\alpha(x^\beta, 0) = S_{jk}(x^\beta, 0) = p(x^\beta, 0) = 0$$
$$(\alpha, \beta = 1, 2). \tag{1.13}$$

2. Numerical Methods of Solution and Their Substantiation. We will use the finite differences method to solve boundary-value problems for the liquid and deformable body. We

introduce two types of difference grids approximating D_1, D_2, and D_t: a three-dimensional grid with constant steps h_1 and h_2: $D_h \subset \{(x_j^1, x_k^2)\colon x_j^1 = x_0^1 + jh_1,\ x_k^2 = x_0^2 + kh_2\}$; a grid on a time layer with the step h_t: $D_t = \{t^n\colon t^n = nh_t,\ n \in Z_+,\ 0 \leqslant nh_t \leqslant \tau\}$. We also construct the additional grids $D_h(0, 1/2)$ and $D_t^{(1/2)}$, having taken the middles of the sides of the initial grids as their nodes. The time grid $D_t^{(1/2)} = \{t^{n+1/2}\colon t^{n+1/2} = (n + 1/2)h_t, t^{n+1/2} < \tau\}$. We use $\mathcal{F}(D)$ to represent the space of real grid functions assigned on D_h and the corresponding boundary-value problems (1.1)-(1.5) for the liquid and (1.5)-(1.13) for the deformable solid. These problems can be represented in generalized divergent form

$$\mathbf{W}_{,t} + \operatorname{div} \mathbf{F}(\mathbf{W}) = \mathbf{S}(\mathbf{W}), \tag{2.1}$$

where $\mathbf{W}$, $\mathbf{F}(\mathbf{W})$, and $\mathbf{S}(\mathbf{W})$ are vectors, while $\mathbf{W} = \mathbf{W}(x^\alpha, t)$, $\mathbf{F} = \{F_1, F_2\}$ and $S = 0$ for the liquid. All of the variables entering into these vectors are henceforth taken as dimensionless. As the characteristic quantities, we take the collision velocity u_0, the size of the incoming flow (drop) of liquid R, and the characteristics of the media $\rho^{(1)}$, $\rho^{(2)}$, $c^{(1)}$, $c^{(2)}$. The conservative form of system (2.1) makes it possible to obtain a solution on the basis of conservative finite-difference approximation schemes (on the above-introduced grid representation) which automatically satisfy the Rankine–Hugoniot relations at shock-wave fronts.

As an example of this approach, below we use the Lachs–Vandroff two-step predictor-corrector scheme [3]. This method includes an explicit time scheme and a central-difference space scheme. The time scheme is obtained by expansion into a Taylor series up to quantities of the second order. In the space scheme, the operators $\partial/\partial x^1$ and $\partial/\partial x^2$ are represented as $\partial/\partial x^\alpha \to \Delta/\Delta x^\alpha$, $\mathcal{F}(D_h) \to \mathcal{F}(D_h(1/2, 0))$, $\frac{\Delta \mathcal{F}}{\Delta x^1}(x^1_{j+1/2}) = (\mathcal{F}(x^1_{j+1}) - \mathcal{F}(x^1_j))/h_1$, etc. Also, the relations $(1/x^1)\cdot\mathcal{F}(D) \to \mathcal{F}(D)$, $(x^1\cdot\mathcal{F})(x_j^1, x_k^2) = x_j^1 \mathcal{F}(x_j^1, x_k^2)$ are valid for the multiplication operators $x^1\cdot$ and $1/x^1\cdot$. Analogous expressions are valid for the operator $(1/x^1\cdot)$. In constructing such schemes, the concept behind the Samarskii method of reference operators [17] is important for reproducing the basic theorems of vector analysis at the discrete level.

As any other scheme of second-order accuracy, the Lachs–Vendroff scheme leads to nonphysical distortions of the solution at the SW fronts and boundaries of contact discontinuity. These distortions cannot be removed (particularly in the latter case) through the use of structural and artificial viscosity. Thus, we use the Boris–Book algorithm [10, 18, 19] for this purpose below. In the first stage – the transport stage – the Lachs–Vendroff method is used with the operator L [3]

$$W_{j,k}^{n+1} = W_{j,k}^n + L \cdot W^n \tag{2.2}$$

(j and k denote the numbers of nodes of the difference grid on D_h and n denotes the moment of time on the grid D_t). The second stage is diffusional and involves the operator D

$$\widetilde{W}_{j,k}^{n+1} = W_{j,k}^{n+1} + D \cdot W^n \tag{2.3}$$

for the values $W_{j,k}^n$ and $W_{j,k}^{n+1}$ corresponding to the given time step. This stage corresponds to linear second-order damping, the operator for which $(DW)_{j,k} = +|\Phi_{j+1/2,k}(W) - \Phi_{j-1/2,k}(W)|$. Here, the flux $\Phi_{j+1/2,k} = (\omega/4)(W_{j+1,k} - W_{j,k})$, while ω is a positive constant, $\omega \sim O(1)$. This approach significantly reduces oscillations at shock-wave fronts and in regions characterized by large gradients of the solution for $\omega \geqslant 1/2$. However, there is also a reduction in the stability of the scheme to $|\sigma| \leqslant (1 - \omega/2)^{1/2}$; for $\omega = 1/2$, $\sigma \leqslant 0.866$.

We will attempt to eliminate the effect of the diffusion stage on the transport stage by also introducing an anti-diffusion operator C(W) with a positive constraint factor q and the constraint operator A(W):

$$(C(\widetilde{W})\cdot W)_{j,k} = -\{[A(\widetilde{W})\,\Phi(W)]_{j+1/2,k} - [(A(\widetilde{W})\Phi(W)]_{j-1/2,k}\}, \tag{2.4}$$

where $|A(\widetilde{W})\Phi(W)|_{j+1/2,k} = q\Phi_{j+1/2,k} \min\{|(\widetilde{W}_{j+2,k} - \widetilde{W}_{j+1,k})|_+,\ (1/q)[(\widetilde{W}_{j,k} - \widetilde{W}_{j-1,k})/\Phi_{j+1/2,k}]_+\}$, while the notation $[a]_+$ has the meaning $[a]_+ = \begin{cases} a, & a \geqslant 0, \\ 0. \end{cases}$

The final form of the flux correction

$$W_{j,k}^{n+1} = \widetilde{W}_{j,k}^{n+1} + C(\widetilde{W}_{j,k}^{n+1})\cdot W_{j,k}^n. \tag{2.5}$$

Choosing from among the solutions of the model problems presented in [18-21, etc.], we took 0.65 as the value of q that is optimum with respect to accuracy and stability. Here, the

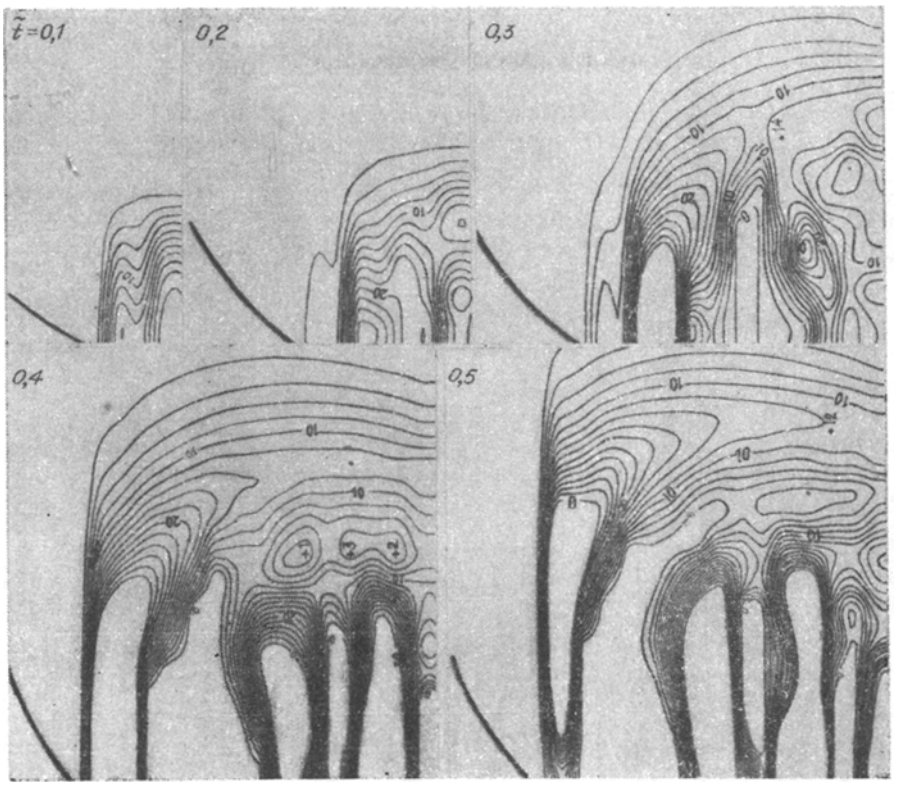

Fig. 1

criterion of stability $|\sigma| \leqslant 1$. Thus, in a unidimensional problem involving contact and shock-wave discontinuities in a shock tube [18], use of the flux-correction method (2.2)-(2.5) with this value reduced the thickness of the shock-wave discontinuity from 4-6 cells of the theoretical grid in the Lachs–Vendroff metod to 1-2 cells. The thickness of the contact discontinuity, meanwhile, was reduced from 6-8 to 4-5 cells. The solutions deviated from the exact values by no more than 1%.

Similar studies of computing schemes have been conducted for other deformable media. The deviations of the solutions at SW fronts were no greater than 3% in the well-known Lamb problem on the incidence of a plane wave on a deformable half-space and in problems involving the impact of deformable bodies flying at different velocities against a rigid obstacle [22, 23]. There was also good agreement of the features of the wave processes occurring during the period of deformation. The use of structural model (1.10)-(1.11) to describe plastically deformed media in such cases makes it possible to obtain closer agreement with empirical results – particularly at high collision velocities – due to fuller accounting of the strain-hardening of the material and its dissipative properties. The accuracy of the calculations was checked by the satisfaction, with a specified relative error, of the energy balance over the entire volume of the deformed medium.

For problems with a free surface, the position of this surface over time is an additional variable which is determined from the solution of the problem. On a Eulerian grid, the new positions of the boundary can be established in accordance with $J^{n+1} = J^n + v^{(1)}_{1j,k}\Delta t$, $K^{n+1} = K^n + v^{(1)}_{2j,k}\Delta t$ – similar to the manner in which this was done in the MAC method [3]. To avoid instability of the free boundary, we will resort to its forced smoothing by a quadratic function of the radius. In the computing process, we first determine the internal hydrodynamic quantities. We then find the change in the boundaries.

The solution of interaction problems was realized in succession: first for the liquid, then, with a time "lag," for the deformable solid. Such an approach has certain advantages [24]. The interaction effect is characterized by conditions (1.5).

3. Impact Interaction of a Body with a Drop Liquid. We use the numerical schemes described above to calculate hydrodynamic flows in a spherical drop of liquid and the deformation and fracture of the surface of a body in a collision occurring at the velocity $M = u_0/c^{(1)} = 0.3$. A drop of the diameter 2R = 2 mm, with a density $\rho^{(1)}$ and sonic velocity $c^{(1)}$ equal to 10^3 kg/m^3 and 1300 m/sec, respectively, collides with a body–half-space made of an

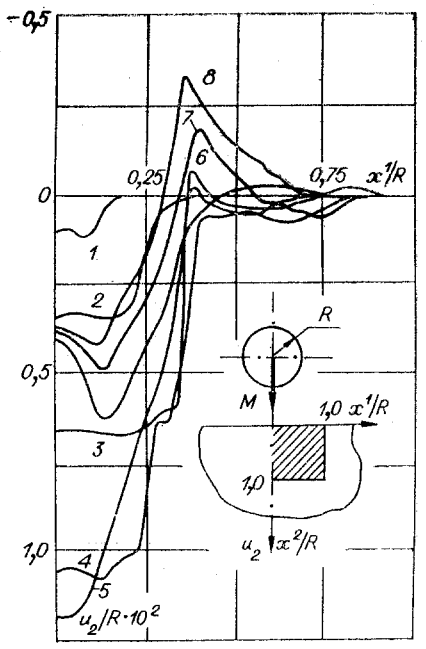

Fig. 2

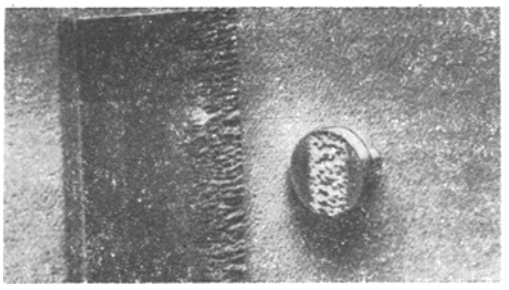

Fig. 3

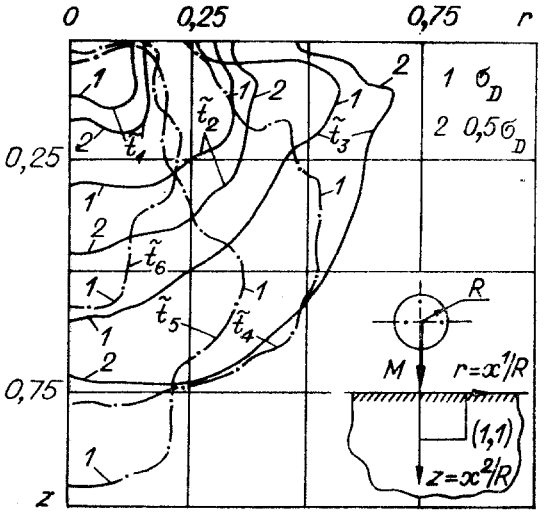

Fig. 4

aluminum alloy having the following properties: shear modulus μ = 26.2 GPa; static yield point σ_0 = 0.36 GPa, with the parameters C and p in Eq. (1.10) equal to 0.0238 and 0.112; density $\rho^{(2)}$ = 2700 kg/m^3; sonic velocity $c^{(2)}$ = 6430 m/sec; Lamé constant λ = 50.8 GPa.

It follows from Fig. 1 that complex hydrodynamic flows take place in the drop. Along with high-pressure regions, cavitation cavities are formed. Figure 1 shows isobars in fractions of $\rho^{(1)}c^2_{(1)}$, where $0.1\,\rho^{(1)}c^2_{(1)} = 10$, for successive moments of time $\tilde{t} = tc^{(1)}/R$ from 0.1 to 0.5. The last moment of time corresponds to the arrival of the SW at the free surface of the drop and the beginning of its intensive dispersion in the horizontal direction. The rate of dispersion agrees well with the experimental value and was reported in [7]. The peak pressures on the surface of the body are somewhat (up to 7%) lower than those obtained in [9] for a rigid surface.

Figure 2 shows changes in the surface of the deformable body in the region of contact with the drop for different moments of time. The final form of the surface is denoted by the number 8 and corresponds to the moment $\tilde{t} = tC/R = 3.0$ from the beginning of loading [$C = ((\lambda + 2\mu)/\rho)^{1/2}$ is the velocity of the longitudinal waves in the body]. The presence of such protuberances around erosional channels is clearly visible on the specimens subjected to drop loading (to the right in Fig. 3). When metal is subjected to repeated loading, the metal forced to the surface is carried off by liquid particles (the damaged surface of a structural element interacting with a drop medium is shown on the left).

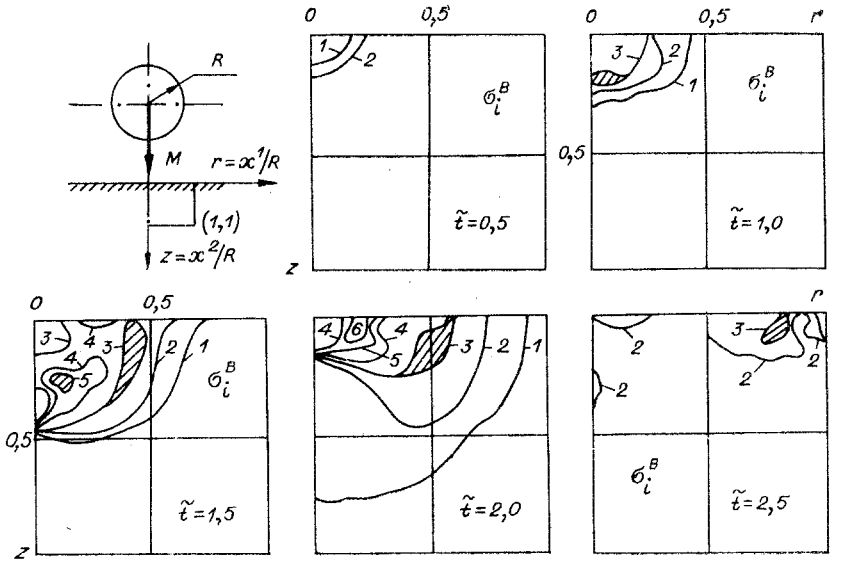

Fig. 5

The character of the stress states which develop in this case differs negligibly from the state obtained when it is assumed that the material behaves elastically [9] – somewhat lower levels of the stress components and the presence of the so-called elastic precursor. The velocity of the latter is greater than the velocity of the plastic wave front in the body. Figure 4 depicts the formation of plastic regions corresponding to the above-mentioned moments of impact interaction. The solid and dot-dash lines represent identical levels of stress intensity. These values are equal to the dynamic yield point and half of this quantity for the same moments of time. The kinetics of the plastic zones depicted by the figure characterizes the regions of the greatest damage, being associated with the highest rates of damage accumulation in the body. Deformation and fracture of the material of the body occur simultaneously and have an effect on one another [25], although it is still not yet possible to account for this effect within the framework of a single mathematical model due to the large difference in the scale of the structures of the body in which these processes take place. The range of scales here is from 10^{-6}-10^{-4} to 10^{2} m or more for actual structures. The porous-body models [26-27] used for this purpose are obviously too coarse. In the present case, the situation is further complicated by the fact that the processes involving deformation and erosional fracture are of a repeating, cyclic character and are generally accompanied by corrosion of the material. Curves of erosional fracture constructed for different drop velocities and sizes as a function of the unit mass lost by the specimen (Fig. 3), time, or the number of collisions also usually include an incubation period, stages of acceleration and deceleration, and a final stage in which the erosion rate is constant. The different stages are in turn characterized by different failure mechanisms. Meanwhile, the beginning of ablation is preceded by the formation of craters [28].

Hypotheses regarding the distribution of drops in a unit volume of the medium and statistical models of fatigue failure are usually introduced to account for the statistical nature of the repeating shock loading and fracture of materials. More accurate results which make it possible to describe features of the erosional fracture curve can be obtained on the basis of a statistical model of ablation [29, 30]. The possibility of the formation of cracks or fracture zones during the initial (incubation) period was not considered in this model.

As our failure criterion, we took the increase in stress intensity past the point corresponding to the intermediate stress σ_i^B in relation to the loading rate (this point being taken with the sign of the maximum tensile stresses). Lines of equal damage in fractions of σ_i^B are shown in Fig. 5. Line 3 is the stress intensity equal to the breaking value σ_i^B for the given moment of loading reckoned from the beginning of the collision of the drop with the deformable body. The hatched region corresponds to the region in which failure can occur.

Thus, we used methods of mathematical modeling that were developed to discover basic laws governing hydrodynamic flows in a drop and deformation processes in a body during their impact interaction. The formation and "collapse" of cavitation zones in the liquid intensifies fracture processes in the body. The deformation processes which take place within the body are quite nonlinear and depend on the loading rate. The character of the processes is

determined more by the accuracy of the description of the cyclic hysteresis properties of the material than by the description of the strain-hardening properties. It is obvious that the above approaches can be generalized to the solution of other interaction problems of practical importance.

LITERATURE CITED

1. "Erosion: Prevention and useful applications," Am. Soc. Test. Mater. Spec. Tech. Publ., No. 664 (1979).
2. J. H. Brunton and M. C. Rochester, "Erosion of solid surfaces by the impact of liquid drops," in: Erosion: Treatise on Materials Science and Technology, Academic Press, New York (1979).
3. P. Rouch, Computational Hydrodynamics [Russian translation], Mir, Moscow (1980).
4. G. Jackson, "Calculation of the collision of a liquid with a solid by means of triangular elements," J. Fluids Eng., 101, No. 2 (1979).
5. G. R. Jonson, "Analysis of elastoplastic impact involving severe distortion," J. Appl. Mech., 98, No. 3 (1976).
6. S. S. Grigoryan (ed.), Dynamcis of Impact [Russian translation], Mir, Moscow (1985).
7. A. L. Gonor and V. A. Yakovlev, "Dynamics of the impact of a drop against a solid surface," Izv. Akad. Nauk SSSR, Mekh. Zhidk. Gaza, No. 1 (1978).
8. V. A. Petushkov, "Numerical methods of studying the hydrodynamic interaction and erosional fracture of solids by a drop liquid," in: Materials of the 6th All-Union Conference on Theoretical and Applied Mechanics, Fan, Tashkent (1986).
9. V. A. Petushkov and M. A. Zaitsev, "Reaction of an elastic body to high-speed shock loading by a drop medium," Mashinovedenie, No. 1 (1989).
10. D. L. Book, J. P. Boris, and K. Hain, "Flux-corrected transport. Part 2: generalization of the method," J. Comput. Phys., 18, No. 2 (1975).
11. Y. C. Fung, Foundations of Solid Mechanics, Prentice-Hall, New Jersey (1965).
12. Ya. B. Zel'dovich and Yu. P. Raizer, Physics of Shock Waves and High-Temperature Hydrodynamic Phenomena [in Russian], Fizmatgiz, Moscow (1966).
13. W. German and R. Lawrence, "Effect of the choice of the model material on the results of calculation of stress-wave propagation," J. Fluid Mech., 100, No. 1 (1978).
14. V. A. Petushkov and S. F. Kashchenko, "Structural modeling of the nonlinear deformation of structures with cracks under cyclic loads," Mashinovedenie, No. 1 (1988).
15. N. Perrone, "Impulsively loaded strain-hardened rate-sensitive rings and tubes," Int. J. Solids Struct., 6, No. 8 (1970).
16. A. N. Romanov, Fracture under Low-Cycle Loading [in Russian], Nauka, Moscow (1988).
17. A. A. Samarskii, V. F. Tishkin, A. P. Favorskii, and N. Yu. Shashkov, "Study of the method of reference operators to construct difference analogs of tensor-analysis operations," Differents. Uravn., 18, No. 7 (1982).
18. G. S. Sod, "A survey of several finite difference methods for systems of nonlinear hyperbolic conservation laws," J. Comput. Phys., 27, No. 1 (1978).
19. H. Niessner and T. Bulaty, "A family of flux-correction methods to avoid overshoot occurring with solutions of unsteady flow problems," 4th GAMM Conf. Numerical Methods in Fluid Mech., Toronto, Canada (1981): Proc.
20. J. Donea, V. Selmin, and L. Quartapelle, "Finite elements schemes for inviscid compressible flows," 8th Intern. Conf. on SMIRT, Brussels, Belgium (1985). Trans. S. 1, Vol. B (1985), pp. 13/3.
21. A. N. Nahavandi, R. R. Pedrido, and R. L. Cloud, "Dynamic analysis of structures with solid-fluid interaction," 4th Intern. Conf. on SMIRT, Calif. (1977), Trans. S. 1, Vol. B (1977), pp. 1/6.
22. V. N. Kukudzhanov, "Numerical solution of non-unidimensional problems of stress-wave propagation in a solid," Soobshch. Prikl. Mat. Vychisl. Tsentr. Akad. Nauk SSSR, 6 (1976).
23. A. N. Bogomolov, V. A. Gorel'skii, S. A. Zelevin, and I. E. Khorev, "Damage to solids of revolution during dynamic contact with a rigid wall," Zh. Prikl. Mekh. Tekh. Fiz., No. 1 (1986).
24. K. C. Park and C. A. Felippa, "Recent developments in coupled field analysis methods," in: Numerical Methods in Coupled Systems, Wiley, New York (1984).
25. V. S. Nikiforovskii and E. I. Shemyakin, Dynamic Fracture of Solids [in Russian], Nauka, Novosibirsk (1979).
26. J. L. Chaboche "Continuous damage mechanics – a tool to describe phenomena before crack initiation," Nucl. Eng. Des., 64, No. 2 (1981).

27. L. K. Romanycheva and A. I. Ruzanov, "Numerical study of cleavage fracture in copper," Zh. Prikl. Mekh. Tekh. Fiz., No. 4 (1982).
28. B. Vyas and C. M. Preece, "Cavitation-induced deformation of aluminum," in: Erosion, Wear, and Interfaces with Corrosion, Am. Soc. Test. Mater. Spec. Tech. Publ., No. 664 (1974).
29. J. Noskievic, "The extended mathematical model of cavitation and erosion by liquid and solid impact," Proc. 6th Intern. Conf. on Erosion by Liquid and Solid Impact, Cambridge, England (1983).
30. H. W. Bargmann, "On the time dependence of the erosion rate – a probabilistic approach to erosion," Teor. Appl. Fract. Mech., 6, No. 3 (1986).